
**Separation Science and Technology**
Publication details, including instructions for authors and subscription information:
http://www.informaworld.com/smpp/title~content=t713708471

# Adsorption of $H_2S$ and $SO_2$ on Bigadiç Clinoptilolite

A. Sirkecioğlu[a]; Y. Altav[a]; A. Erdem-Şenatalar[a]
[a] DEPARTMENT OF CHEMICAL ENGINEERING, ISTANBUL TECHNICAL UNIVERSITY, MASLAK, ISTANBUL, TURKEY

**To cite this Article** Sirkecioğlu, A. , Altav, Y. and Erdem-Şenatalar, A.(1995) 'Adsorption of $H_2S$ and $SO_2$ on Bigadiç Clinoptilolite', Separation Science and Technology, 30: 13, 2747 — 2762
**To link to this Article: DOI:** 10.1080/01496399508013713
**URL:** http://dx.doi.org/10.1080/01496399508013713

SEPARATION SCIENCE AND TECHNOLOGY, **30**(13), pp. 2747–2762, 1995

# Adsorption of $H_2S$ and $SO_2$ on Bigadiç Clinoptilolite

A. SIRKECIOĞLU, Y. ALTAV, and A. ERDEM-ŞENATALAR*
DEPARTMENT OF CHEMICAL ENGINEERING
ISTANBUL TECHNICAL UNIVERSITY
80626 MASLAK, ISTANBUL, TURKEY



## ABSTRACT

$H_2S$ and $SO_2$ adsorption isotherms of Bigadiç clinoptilolite and its Na-, K-, Ca-, and H-enriched forms were determined in the 0 to 100 kPa range at 25°C by using a constant volume adsorption system. Langmuir, Freundlich, Dubinin–Radushkevich (D-R), and Dubinin–Astakhov (D-A) models were applied to the isotherm data. Higher adsorption capacities and a larger increase in the amount adsorbed at higher pressures were observed for $SO_2$, in agreement with its higher permanent dipole moment, resulting in stronger ion–dipole and dipole–dipole interactions for this molecule. The Ca-form exhibited a molecular sieving behavior for both gases, originating from the channel blockage caused by the cation locations in the sample. The highest capacities for both gases were obtained with the sample in its H-form, followed by the Na- and K-forms for $SO_2$, parallel to the decrease in the electronegativity and ionic potential and the increase in the polarizability of the cation. In the case of $H_2S$, the H-form was followed by the K-form, but the Na-form yielded very low adsorption capacities. Initial dissociative adsorption of $H_2S$ on certain Na sites to yield SH and OH species is thought to contribute to a more effective blocking of the channels, which were already partially blocked in this sample. Of the isotherm models tested, the D-A model explained the variations in the data better than either the Freundlich or D-R models. For the cation-gas combinations with a lower extent of channel blockage though, the Langmuir model was somewhat more representative. Lower $E$ and $n$ values were obtained from the D-A model for $H_2S$ on the Na-form, which may be related to the lower extent of micropore adsorption and to the presence of blocked, almost dead-end shorter channel segments in the sample. Pore volumes close to the theoretical value were estimated from the D-A parameters for $SO_2$ adsorption.

* To whom correspondence should be addressed at Department of Chemical Engineering, Istanbul Technical University, 80626 Maslak, Istanbul, Turkey. Telephone: 90-212-285 68 96; FAX: 90-212-285 29 25; E-mail: KMERDEM@CC.ITU.EDU.TR

*Key Words.* Clinoptilolite; Natural zeolite; Adsorption; $H_2S$; $SO_2$; Dubinin–Astakhov

## INTRODUCTION

Clinoptilolite is a silica-rich natural zeolite that has abundant and mineable deposits in many countries (1). Although hindered by the variation in purity and composition of the natural deposits, there has still been some interest in the use of clinoptilolite as an adsorbent for the removal of $CO_2$, $H_2S$, $N_2$, and $H_2O$ from natural gas or other hydrocarbon streams (2–7), $SO_2$ from flue gases (8), $NH_3$ from coal gasification products (9), for air separations to produce $N_2$ or $O_2$ (10, 11), and for other gas separations such as $H_2$ recovery from $H_2/N_2$ mixtures (12).

Recently, clinoptilolite was shown to have a much greater potential for the separation of gas mixtures than previously recognized (5–7). Cation location was observed to be far more important to channel blocking than size or number of the cations, and this property was successfully utilized to tailor clinoptilolite for the kinetic separation of $N_2/CH_4$ mixtures.



Western Anatolia is rich in clinoptilolite formations (13). One of the most important occurrences, with a reserve estimated to approach 2 billion tons, is found in the Bigadiç basin (14). The zeolite in the tuffs was classified as Ca-rich clinoptilolite, based on its thermal stability and composition (15). The reserve has two visibly different zones, which also differ in their thermal stability, cationic composition, and ion-exchange behavior (16). The coarse-grained tuffs which are located at the bottom zone were observed to be thermally more stable than the fine-grained tuffs located on top. Zeolite contents of the samples taken from known locations in the reserve were determined not to fall below 55%, except for those samples from the border regions. Most of the samples had clinoptilolite contents of more than 80% (15).

$CO_2$ adsorption was observed to be strongly dependent on the cation type and zeolite content for Bigadiç samples (17–19). High separation factors for $CO_2/N_2$, $NO/N_2$, and $CO/N_2$ were predicted with a representative sample taken from the coarse-grained zone without any pretreatment (20). $SO_2$ was shown by ESR to be reduced by CO or $H_2S$ on the same sample (21).

We report here the results of a study on the adsorption of two sulfur compounds, $H_2S$ and $SO_2$, on Bigadiç clinoptilolite and its Na-, K-, Ca-, and H-enriched forms. Removal of $H_2S$ and $SO_2$ from natural gas, air, and hydrocarbon feedstreams is known to be an important separation

in the oil, gas, and chemical process industries and for environmental purposes.

## EXPERIMENTAL

A representative coarse-grained sample with a clinoptilolite content of about 95%, similar to those used in previous studies (20, 21), was crushed and sieved to obtain the 90–150 μm fraction, which was then washed with distilled water for 24 hours in a Soxhlet extractor for the removal of water-soluble impurities. Na-, K-, and Ca-enriched forms of the sample were prepared by repeated ion-exchange treatments in 1 M solutions of the respective chloride salts at 80°C for 5 hours. One hundred milliliters of the exchange solution was used per gram of zeolite, and the treatments were repeated three times for the preparation of each form. A portion of the Na-enriched sample was then converted to the $NH_4^+$-form in a 1 M solution of $NH_4Cl$, again at 80°C for 5 hours, which in turn was calcined to obtain the H-form. Chemical analyses were performed by standard techniques using wet chemical methods for Si, Ca, and Mg, atomic absorption spectroscopy for Al and Fe, and flame photometry for Na and K.

Adsorption experiments were carried out in a constant volume adsorption system. $H_2S$ and $SO_2$ isotherms of the samples in the 0 to 100 kPa range at 25°C were determined. A minimum of 15 minutes at the same pressure was allowed for each equilibrium data point. All samples were heated at a rate of 2°C/min to 400°C and were activated at this temperature and $10^{-5}$ mbar pressure for 6 hours prior to the adsorption experiments.

Langmuir, Freundlich, Dubinin–Radushkevich, and Dubinin–Astakhov models were applied to the isotherm data (22). The saturation P–T relationship was approximated using the Clausius–Clapeyron equation between the normal boiling and critical temperatures, and this relationship was then extrapolated to determine a pseudosaturation pressure at the temperature of the measured isotherm for the application of the Dubinin–Astakhov equation above the critical temperature, as has been detailed previously (5). The quality of fits was checked by statistical methods, and model parameters were calculated for each case.

## RESULTS AND DISCUSSION

Chemical analyses of the original sample and its Na-, K-, Ca-, and H-enriched forms are given in Table 1. Since the original sample is known to be rich in its clinoptilolite content, unit cell compositions based on 72

TABLE 1
Chemical Analyses of the Original Sample and Its Cation-Enriched Forms

| Sample | % Oxide | | | | | | |
|---|---|---|---|---|---|---|---|
| | $SiO_2$ | $Al_2O_3$ | $Fe_2O_3$ | $Na_2O$ | $K_2O$ | CaO | MgO |
| Clinoptilolite | 59.97 | 12.69 | 1.27 | 0.32 | 2.41 | 2.87 | 1.99 |
| Na-clinoptilolite | 62.11 | 12.50 | 0.59 | 6.01 | 0.26 | 0.66 | 0.31 |
| K-clinoptilolite | 63.30 | 11.93 | 0.56 | 0.26 | 7.18 | 0.38 | 0.18 |
| Ca-clinoptilolite | 62.68 | 12.62 | 0.77 | 1.15 | 0.37 | 4.78 | 1.25 |
| H-clinoptilolite | 63.83 | 12.75 | 0.96 | 0.66 | 0.24 | 0.43 | 0.26 |

oxygens are also calculated for convenience in comparisons. The values are listed in Table 2.

The increase in the Si/Al ratios and the decrease in the iron contents of the ion-exchanged forms may be related to the presence of soluble aluminum and iron salts in the original sample. More than 80% of the cation equivalents consisted of Na and K in the respective cation forms, whereas this value was about 61% for the Ca-form. More than 22% of the cation equivalents remained to arise from Mg in this sample.

$H_2S$ and $SO_2$ adsorption isotherms for the original sample and its Na-, K-, Ca-, and H-enriched forms are shown in Figs. 1 and 2, respectively. The $SO_2$ isotherm for the Ca-form is not given in Fig. 2 because this sample practically did not adsorb within the accuracy of our experiments.

The experimental adsorption capacities at 100 kPa, which are also listed in Table 6, are higher than those reported for various clinoptilolite samples from Sheaville, Alaska and Hungary (23, 24).

Table 3 lists some of the physical properties of the gases used. As can be seen from the table, their kinetic diameters are similar and both $SO_2$ and $H_2S$ have permanent dipole moments. At low pressures, therefore,

TABLE 2
Unit Cell Compositions of the Samples

| Sample | Si | Al | Fe | Na | K | Ca | Mg | Si/Al |
|---|---|---|---|---|---|---|---|---|
| Clinoptilolite | 28.48 | 7.10 | 0.45 | 0.29 | 1.46 | 1.46 | 1.41 | 4.01 |
| Na-clinoptilolite | 29.01 | 6.89 | 0.21 | 5.45 | 0.15 | 0.33 | 0.22 | 4.21 |
| K-clinoptilolite | 29.45 | 6.67 | 0.20 | 0.24 | 4.34 | 0.19 | 0.13 | 4.43 |
| Ca-clinoptilolite | 28.76 | 6.83 | 0.27 | 1.02 | 0.22 | 2.35 | 0.86 | 4.21 |
| H-clinoptilolite | 30.05 | 7.08 | 0.34 | 0.60 | 0.14 | 0.21 | 0.18 | 4.24 |

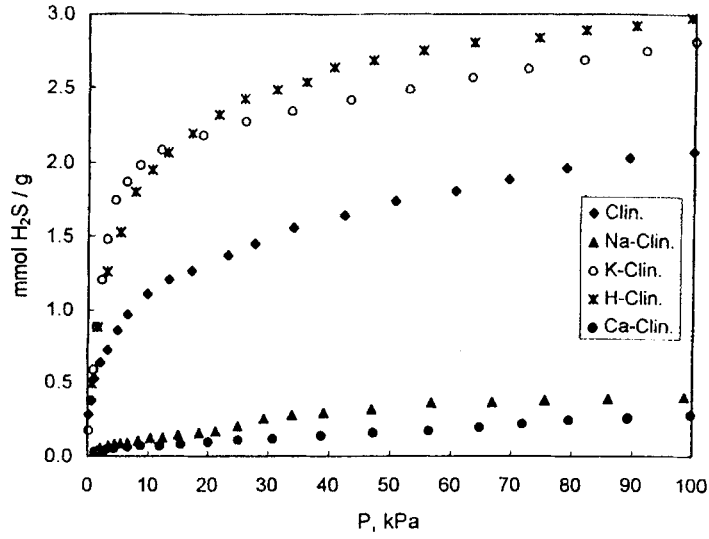


FIG. 1 $H_2S$ adsorption isotherms of clinoptilolite and its cation-enriched forms.

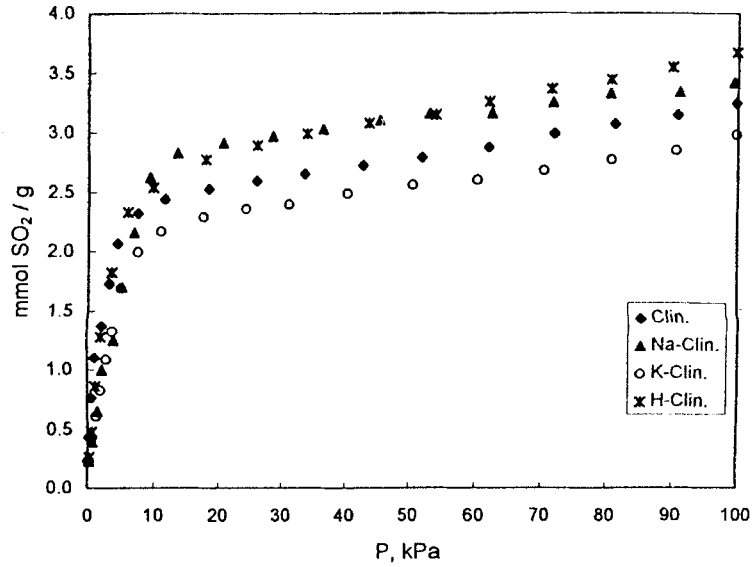


FIG. 2 $SO_2$ adsorption isotherms of clinoptilolite and its cation-enriched forms.

TABLE 3
Some Physical Properties of $H_2S$ and $SO_2$ (25)

| Molecule | Dipole (debye) | Polarizability (Å$^3$) | Ionization potential (V) | Kinetic diameter (Å) |
|---|---|---|---|---|
| $H_2S$ | 0.97 | 3.78, 3.95 | 10.40 | 3.6 |
| $SO_2$ | 1.63 | 3.72, 4.28 | 12.34 | 3.6 |

ion–dipole interaction between the gas molecules and the adsorbent is dominant, the potential energy of which is proportional to the charge of the ion on the solid surface and the dipole moment of the gas molecule. This explains the higher adsorption capacities observed for $SO_2$, the dipole moment of which is also significantly higher. As the pressure is increased, dipole–dipole interaction between the adsorbed molecules and those in the gas phase starts to gain importance, which is also a function of the dipole moment but is weaker than the ion–dipole interaction. It is this dipole–dipole interaction that explains the larger increase in the amount of adsorbed $SO_2$ with respect to $H_2S$ at higher pressures.

The adsorption capacities of the samples at 100 kPa decreased in the order H-form > K-form > Na-form > Ca-form for $H_2S$ and H-form > Na-form > K-form > Ca-form for $SO_2$ adsorptions. The capacities of the original clinoptilolite lie somewhere in between, which can be explained by its mixed cationic composition. Similar orders were reported for $H_2S$ and $SO_2$ adsorptions by Zarchy et al. (4) who used clinoptilolite at 423 K and by Kallo et al. (24) with mordenite at 293 K.

The sample in its Ca-form yielded the lowest capacities for the adsorption of both $H_2S$ and $SO_2$. Ca-clinoptilolite samples have also been observed to have the lowest adsorption capacities for $CO_2$ (19) and $N_2$ and $CH_4$ (5) gases.

The low capacities obtained with the Ca-forms originate from the unique pore geometry coupled with the cation locations in this zeolite, as was demonstrated elegantly by Ackley and Yang (6). There are three intersecting channel systems lying in two dimensions in the monoclinic clinoptilolite structure. These are the 10- and 8-membered ring channels (channels A and B, respectively) lying parallel to each other and the *c* axis of the unit cell, and the 8-membered ring channel (channel C) lying parallel to the *a* axis and intersecting both the A and B channels (26). Of the cation positions M(1)–M(4), which were shown to be present in the structure, Na and Ca are known to occupy the M(1) and M(2) sites, located at the

intersections of the A and B channels, respectively, with channel C. The probability of the occupation of the M(2) site by Ca was reported to be higher (26). Mg and K, on the other hand, were observed to occupy the M(4) and M(3) sites, which are located at the symmetry center of the 10-membered ring channel A and in the middle of the 8-membered ring channel C, respectively. A unit cell is known to contain only four combined M(1) and M(2) sites, four M(3) sites, and two M(4) sites. M(1)–M(3) and M(1)–M(4) are forbidden pairs and cannot be simultaneously occupied in a given unit cell (26). The channel blockage matrix developed, accordingly, for $CH_4$ and $N_2$ diffusion in ion-exchanged clinoptilolites (6) is applicable to our case too, since $H_2S$ and $SO_2$ molecules are also of similar size. A small amount of Mg was argued to be sufficient to effectively block the 10-membered ring channel, especially if it was located near the crystal surface at M(4) sites. The Ca-enriched sample used in this study contained a significant amount of Mg, which consisted of about 22% of the cation equivalents as mentioned above. Since channels B and C were already totally and partially blocked, respectively, because of the presence of almost 4Ca + Na cations at the M(2) sites in the sample, it is understandable for this cation form to exhibit the observed molecular sieving behavior.

The highest capacities for both gases were obtained with the sample in its H-form, except for a narrow pressure range close to the low pressure end, causing the isotherms on H-forms to be less rectangular. The exact locations of H ions in the channels are not known (5), but apparently an open structure results with H ions replacing about 80% of the cation equivalents. As can be seen from Table 4, which lists some of the physical properties of the cations, H has the highest electronegativity and ionic potential values, which in turn are known to be important in determining the gas–solid interaction energies and hence the equilibrium adsorption capacities (27). The presence of surface OH groups in H-zeolites and their

TABLE 4
Some Physical Properties of the Cations (31)

| Cation | Sanderson electronegativity | Ionic potential (eV) | Polarizability ($Å^3$) |
|---|---|---|---|
| H | 2.31 | 13.60 | 0.67 |
| Na | 0.85 | 5.139 | 23.6 |
| K | 0.74 | 4.341 | 43.4 |
| Ca | 1.06 | 6.113 | 22.8 |

capability of H-bonding to gases like $H_2S$ (28–30) might have also played a role.

The adsorption capacities for $SO_2$ decrease in the order of H-form > Na-form > K-form, parallel to the decrease in the electronegativity and the ionic potential and to the increase in the polarizability of the cation. In the case of $H_2S$, the H-form is followed by the K-form, but the Na-form yielded very low adsorption capacities which were slightly higher than those obtained with the Ca-form.

The explanation of this behavior must lie in a unique pore blocking that takes place during the adsorption of $H_2S$ on Na-clinoptilolite. $H_2S$ was shown by the ESR technique to dissociate at room temperature on an activated clinoptilolite sample similar to the original sample used in this study (21). An ESR signal was observed due to the interaction of $SH^-$ ions formed by the ionization of $H_2S$ with certain sites of the clinoptilolite. Dissociative adsorption of $H_2S$ and formation of SH and OH species have also been reported for NaY (29) and NaA (30) type zeolites, but were not observed on NaCa A (30). $Na^+$ cations at certain sites on the walls of the cages were thought to be the centers of dissociative $H_2S$ adsorption in both cases. Similarly, in our case, a certain concentration of such Na-sites, on which $H_2S$ is dissociatively adsorbed, might have contributed to more effective blocking of the channel system. Channel B is already totally blocked and channels A and C are partially blocked in the Na-form, which has a total of about 6 Na and Ca cations (6). The presence of initially chemisorbed $H_2S$ species at a certain concentration must have resulted in an almost dead-end channel system, preventing further diffusion of $H_2S$ molecules into the clinoptilolite pores, most of which are not much larger than the gas molecules.

Langmuir, Freundlich, Dubinin–Radushkevich (D-R), and Dubinin–Astakhov (D-A) models were applied to the isotherm data in the 0 to 100 kPa range. The theoretical curves obtained by the application of the models can be compared with the experimental data in Figs. 3 and 4 for $H_2S$ and $SO_2$ adsorptions, respectively. The D-A model explains the variation in the data better than either the Freundlich or D-R models in the 0 to 100 kPa range for both gases and all cation forms, as can also be seen from the determination coefficients ($r^2$) of the correlations listed in Table 5. The D-A model, which is an improved version of the D-R formulation, was derived to be valid for a larger pressure range than most isotherm models, whereas the Freundlich isotherm is known to be valid for a narrow range with low adsorbate pressures (22). For some cation-form–gas combinations though, the Langmuir model was somewhat more representative.

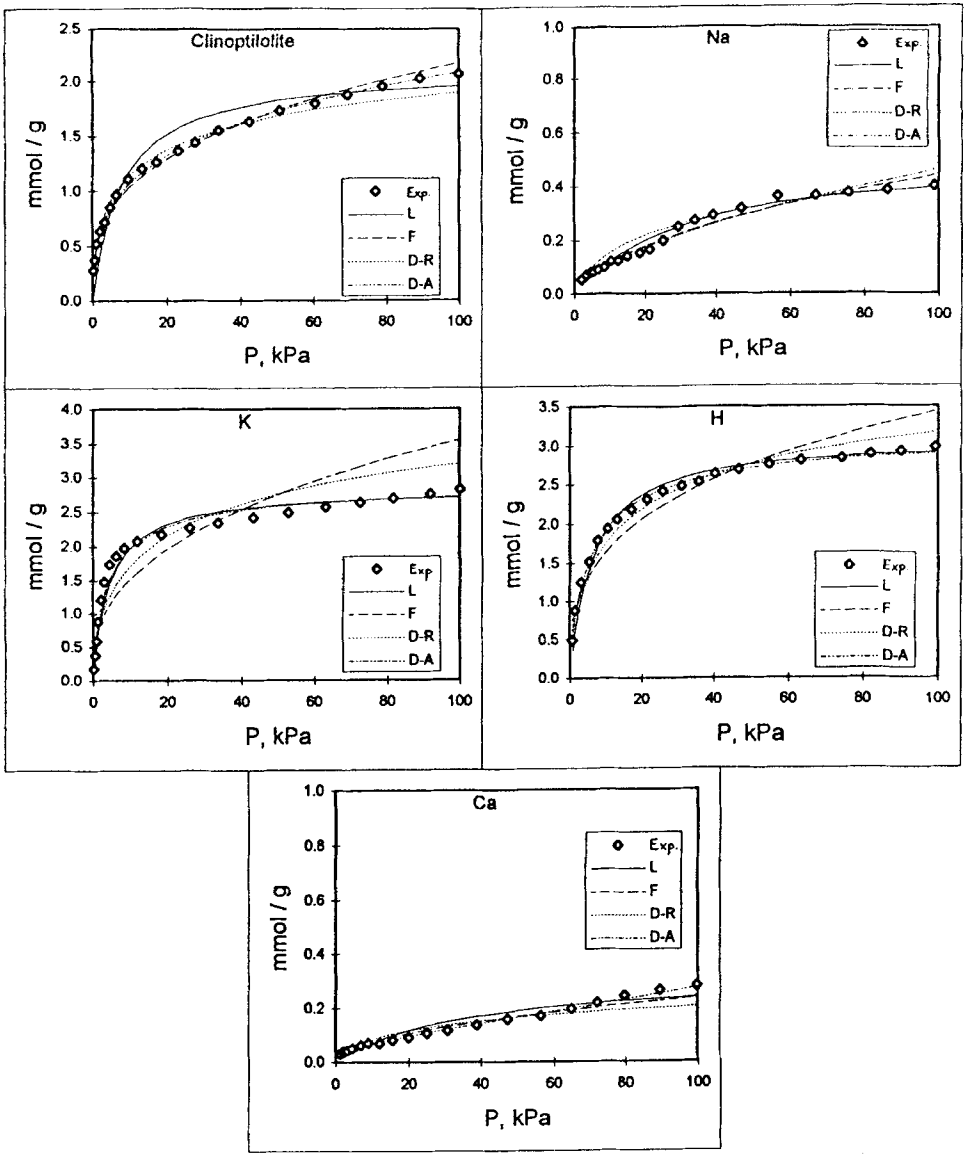


FIG. 3 Model isotherms for $H_2S$ adsorption.

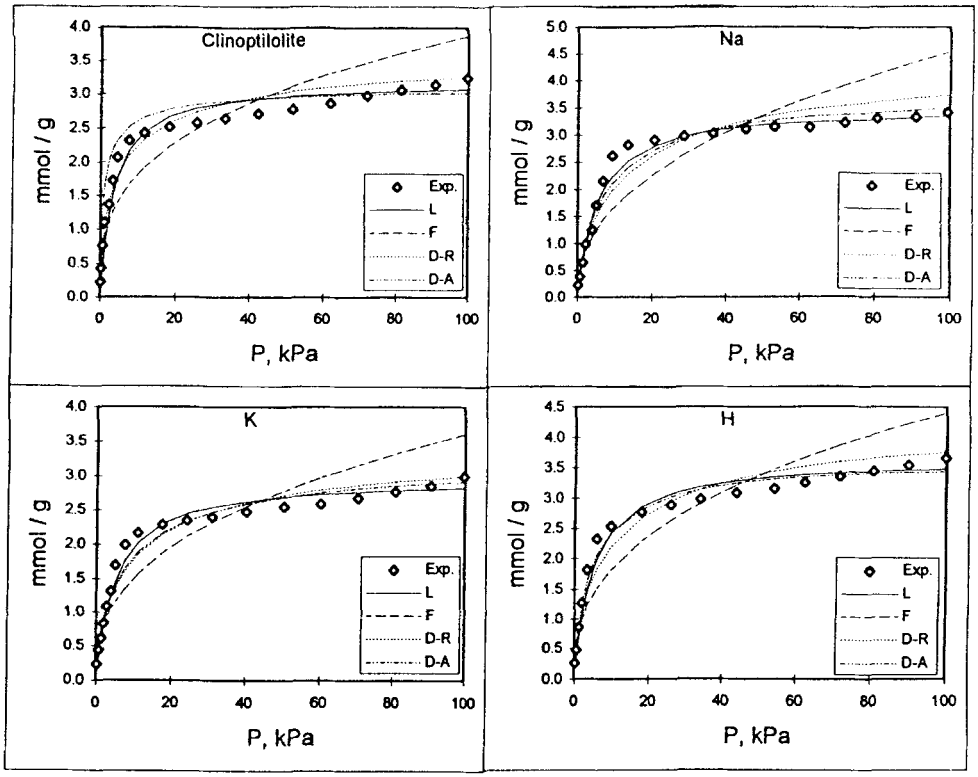


FIG. 4 Model isotherms for $SO_2$ adsorption.



TABLE 5
Determination Coefficients ($r^2$) of the Correlations

| Gas | Sample | Langmuir | Freundlich | D-R | D-A |
|---|---|---|---|---|---|
| $H_2S$ | Clinoptilolite | 0.9861 | 0.9942 | 0.9856 | 0.9975 |
| | Na-clinoptilolite | 0.9402 | 0.9820 | 0.9578 | 0.9827 |
| | K-clinoptilolite | 0.9970 | 0.8408 | 0.9328 | 0.9866 |
| | Ca-clinoptilolite | 0.8258 | 0.9715 | 0.9183 | 0.9946 |
| | H-clinoptilolite | 0.9984 | 0.9120 | 0.9723 | 0.9963 |
| $SO_2$ | Clinoptilolite | 0.9947 | 0.8937 | 0.9849 | 0.9949 |
| | Na-clinoptilolite | 0.9986 | 0.8838 | 0.9759 | 0.9833 |
| | K-clinoptilolite | 0.9965 | 0.9038 | 0.9778 | 0.9791 |
| | H-clinoptilolite | 0.9955 | 0.8888 | 0.9771 | 0.9930 |

The D-A model was more powerful than the Langmuir model for cases with a higher extent of channel blockage, such as adsorption of both gases on the original clinoptilolite and $H_2S$ on the Na-form. On the other hand, the Langmuir model was seen to represent the isotherm data very well, especially for the adsorption of both gases on the H- and K-forms and for $SO_2$ on the Na-form.

The monolayer adsorption capacities estimated with the Langmuir model are in accordance with the experimental capacities, and they follow the same order of cation forms as can be seen from the $q_{Lang}$ values listed in Table 6.

In general, the model with the most sufficient explanation power for all cases is the D-A model. The determination coefficients with this model did not fall below about 0.98 in any case.

Adsorption in the channels of clinoptilolite, which are slightly larger than the gas molecules, is strongly affected by the internal electrostatic fields, and the D-A model based on volume filling of the pores seems to account for this pore–adsorbate interaction sufficiently well. The model isotherm is given by the following equation (32):

$$q = q_0 \exp[-(A/E)^n]$$

where $q$ is the amount of gas adsorbed at pressure $P$, $q_0$ is the limiting adsorption value, $E$ is the characteristic free energy of adsorption, and $n$ is a structural parameter. The differential molar work of adsorption is defined as

$$A = RT \ln (f_s/P)$$

A hypothetical reference state ($P_s$, $T$) was established by estimating the



TABLE 6
Experimental Capacities at 100 kPa and the Model Parameters and Micropore Volumes of the Samples

| Gas | Sample | $q_{exp}$ (mmol/g) | $q_{,Lang}$ (mmol/g) | $q_{0,D\text{-}A}$ (mmol/g) | $n$ | $E$ (kJ/mol) | $W_0(T_b)$ ($cm^3/g$) |
|---|---|---|---|---|---|---|---|
| $H_2S$ | Clinoptilolite | 2.08 | 2.12 | 3.33 | 1.35 | 10.74 | 0.102 |
| | Na-clinoptilolite | 0.40 | 0.54 | 3.31 | 0.80 | 2.62 | 0.102 |
| | K-clinoptilolite | 2.82 | 2.82 | 2.78 | 3.65 | 16.06 | 0.086 |
| | H-clinoptilolite | 2.98 | 3.09 | 3.07 | 3.25 | 15.21 | 0.100 |
| $SO_2$ | Clinoptilolite | 3.25 | 3.18 | 3.05 | 2.55 | 13.17 | 0.137 |
| | Na-clinoptilolite | 3.44 | 3.53 | 3.58 | 2.40 | 10.41 | 0.161 |
| | K-clinoptilolite | 2.99 | 2.96 | 3.03 | 2.15 | 11.04 | 0.136 |
| | H-clinoptilolite | 3.67 | 3.66 | 3.50 | 2.70 | 12.00 | 0.157 |

pseudosaturation pressure ($P_s$) at the temperature of the experimental isotherm, as mentioned in the previous section, to allow for the computation of the fugacity, $f_s$, and the differential molar work of adsorption, $A$.

The limiting adsorption capacities, $q_0$, characteristic energies, $E$, and geometric factors, $n$, all calculated by application of the D-A model to the experimental isotherm data, are given in Table 6, which also lists the pore volumes, $W_0(T_b)$. Values for the Ca-form exhibiting a molecular sieving behavior are not included in the table since the $E$ and $n$ values were almost zero and therefore $q_0$ is meaningless. Pore volumes were calculated from the limiting adsorption values at the normal boiling temperature, $q_0(T_b)$, assuming that the density of the adsorbate is the same as that of the bulk liquid ($\rho_b$) at its boiling point, as follows:

$$W_0(T_b) = \frac{q_0(T_b)M_w}{\rho_b}$$

Limiting adsorption values at the normal boiling temperature, $q_0(T_b)$, are calculated from $q_0(T)$ determined from the model and the thermal coefficient of limiting adsorption, $\alpha$, using the following relationship (32).

$$q_0(T_b) = q_0(T) \exp[-\alpha(T_b - T)]$$

The thermal coefficient of the limiting adsorption, $\alpha$, is defined as

$$\alpha = -\frac{d \ln q_0}{dT} = \frac{\ln(\rho_b/\rho_c^*)}{T_c - T_b}$$

where $\rho_c^*$ is the sorbate density at the critical temperature, which was calculated using the van der Waals covolume (32).

The characteristic energies for $SO_2$ adsorption on Na-, K-, and H-forms vary in the narrow range of 10.4–12.0 kJ/mol. The interaction between the adsorbate and $SO_2$ molecules with their permanent dipoles does not seem to depend strongly on the cation type according to the D-A model, which is also in accordance with the close adsorption capacity values. A similar observation can be made for $H_2S$ adsorption on the K- and H-forms, the $E$ values for which are calculated to be 16.1 and 15.2 kJ/mol, respectively. $CO_2$ adsorption was carried out on the same samples in another study (19), and the D-A characteristic energies were calculated to be 15.4, 21.6, and 27.0 kJ/mol for the H-, Na-, and K-forms, respectively. The wide range of $E$ values observed in this case is related to the high cation selectivity of quadrupolar $CO_2$ resulting from the pronounced differences in its interaction with different cations.

The original clinoptilolite and especially its Na-form gave much lower $E$ values for $H_2S$ adsorption, in agreement with their low $n$ values, as will be discussed below.

Though its exact physical significance remains unclear, the $n$ parameter is argued to increase with decreasing size of the pores relative to the size of the adsorbate (33), resulting in a loss of degrees of freedom by the adsorbate. For the H- and K-forms the $n$ values are seen to be higher for $H_2S$ than for $SO_2$ adsorption. The original clinoptilolite sample and especially its Na-form yielded much lower $n$ values for $H_2S$ adsorption. The experimental capacities were also much lower in these cases. Although one tends to think of a more restricted adsorption taking place in these samples, the smaller values of $n$ and $E$ may be related to a lower extent of micropore adsorption into the depths of the crystals, resulting from the presence of blocked, almost dead-end, shorter channel segments.

Pore volumes calculated from the $SO_2$ adsorption data for the original sample and its K-form are in accordance with the values calculated from $CH_4$ and $n$-hexane adsorption, which were reported to be 0.135 and 0.129 $cm^3/g$, respectively (5). Water desorption data on a Na-clinoptilolite sample has yielded a similar value (34). Higher values were obtained from the $SO_2$ adsorption data for the H- and Na-forms in this study. These values are closer to the theoretical pore volume of 0.186 $cm^3/g$ calculated for Na-clinoptilolite by Barrer (35), assuming 24 water molecules/unit cell. Pore volumes calculated from the $H_2S$ adsorption data, on the other hand, are somewhat smaller. It is interesting to note that exclusion of $H_2S$ by the Na-form is not evidenced by a lower pore volume, against our expectations. On the contrary, the D-A model is seen to estimate a high limiting adsorption capacity at saturation ($q_0$) for this sample, similar to the others, which is not achieved under the experimental conditions applied.



## CONCLUSIONS

Adsorption of $H_2S$ and $SO_2$ on Bigadiç clinoptilolite and its Na-, K-, Ca-, and H-enriched forms was studied in a constant volume adsorption system. $H_2S$ and $SO_2$ isotherms of the samples in the 0 to 100 kPa range at 25°C were determined, and Langmuir, Freundlich, Dubinin–Radushkevich, and Dubinin–Astakhov models were applied to the isotherm data.

Higher adsorption capacities were observed for $SO_2$, in agreement with its higher permanent dipole moment. There was also a larger increase in the amount of adsorbed $SO_2$ at higher pressures, arising from the stronger dipole–dipole interaction between $SO_2$ molecules.

The Ca-form did not adsorb $SO_2$ and yielded very low capacities for $H_2S$, originating from channel blockage in the sample. The highest capacities for both gases were obtained with the sample in its H-form, which was followed by the Na- and K-forms for $SO_2$, parallel to the decrease in the electronegativity and ionic potential and the increase in the polariz-

ability of the cation. In the case of $H_2S$, the H-form was followed by the K-form, but the Na-form yielded very low adsorption capacities. The initial dissociative adsorption of $H_2S$ on certain Na sites to yield SH and OH species is thought to contribute to effective blocking of the channel system, which was already partially blocked in this sample.

Of the isotherm models applied, the Dubinin–Astakhov model was found to explain the variation in the data better than either the Freundlich or Dubinin–Radushkevich models in the 0 to 100 kPa range for both gases and all cation forms. For cation–gas combinations with a lower extent of channel blockage though, the Langmuir model was more representative. Lower $E$ and $n$ values were obtained from the application of the Dubinin–Astakhov model to the adsorption of $H_2S$ on the Na-form, which may be related to a lower extent of micropore adsorption into the depths of the crystals, resulting from the presence of blocked, almost dead-end, shorter channel segments. A value of about 0.16 $cm^3/g$ for the pore volume was estimated from the Dubinin–Astakhov model calculations applied to $SO_2$ adsorption data on H- and Na-forms, which is close to 0.186 $cm^3/g$, the theoretical value for clinoptilolite.



## REFERENCES


1. F. A. Mumpton, "Development of Uses for Natural Zeolites: A Critical Commentary," in *Occurrence, Properties and Utilization of Natural Zeolites* (D. Kallo and H. S. Sherry, Eds.), Akademiai Kiado, Budapest, 1988, p. 333.
2. C. C. Chao, "Selective Adsorption on Magnesium-Containing Clinoptilolites," US Patent 4,964,889 (1990).
3. C. C. Chao, and H. Rastelli, "Process for Purification of Hydrocarbons," US Patent 5,019,667 (1991).
4. A. S. Zarchy, R. Correia, and C. C. Chao, "Process for the Adsorption of Hydrogen Sulfide with Clinoptilolite Molecular Sieves," US Patent 5,164,076 (1992).
5. M. W. Ackley and R. T. Yang, "Adsorption Characteristics of High Exchanged Clinoptilolites," *Ind. Eng. Chem. Res.*, *30*, 2523 (1991).
6. M. W. Ackley and R. T. Yang, "Diffusion in Ion-Exchanged Clinoptilolites," *AIChE J.*, *37*(11), 1645 (1991).
7. M. W. Ackley, R. R. Giese, and R. T. Yang, "Clinoptilolite: Untapped Potential for Kinetic Gas Separations," *Zeolites*, *12*, 780 (1992).
8. K. Torii, "Utilization of Natural Zeolites in Japan," in *Natural Zeolites* (L. B. Sand and F. A. Mumpton, Eds.), Pergamon Press, Oxford, 1978, p. 441.
9. D. T. Hayhurst, "The Potential Use of Natural Zeolites for Ammonia Removal during Coal-Gasification," in *Natural Zeolites* (L. B. Sand and F. A. Mumpton, Eds.), Pergamon Press, Oxford, 1978, p. 503.
10. I. M. Galabova, G. A. Haralampiev, and B. Alexiev, "Oxygen Enrichment of Air Using Bulgarian Clinoptilolite," in *Natural Zeolites* (L. B. Sand and F. A. Mumpton, Eds.), Pergamon Press, Oxford, 1978, p. 431.
11. I. M. Galabova and G. A. Haralampiev, "Oxygen Enrichment of Air on Alkaline Forms

of Clinoptilolite," in *The Properties and Applications of Zeolites* (Spec. Publ. 33), (R. P. Townsend, Ed.), Chemical Society, London, 1980, p. 121.
12. M. Abrudean, A. Baldea, and D. Axente, "Hydrogen Recovery from Hydrogen–Nitrogen Mixtures by Selective Adsorption on Natural Clinoptilolite," *Zeolites*, *5*, 211 (1985).
13. G. Ataman, "Zeolite Occurrences in Western Anatolia," *Earth Sci.*, *3*, 85 (1977) (in Turkish).
14. O. Baysal, N. Gündoğdu, A. Temel, and F. Öner, *Geological Investigation of the Zeolite Formations in Bigadiç*, Project Report, Hacettepe University, YUVAM, 85-2, Ankara, 1986 (in Turkish).
15. A. Sirkecioğlu, F. Esenli, I. Kumbasar, R. H. Eren, and A. Erdem-Şenatalar, "Mineralogical and Chemical Properties of Bigadic Clinoptilolite," in *Proceedings of the International Earth Science Congress on Aegean Regions (IESCA), 1–6 October 1990, Izmir*, Vol. 1 (M. Y. Savaşçın and A. H. Eronat, Eds.), 1991, p. 291.
16. A. Erdem-Şenatalar, A. Sirkecioğlu, I. Güray, F. Esenli, and I. Kumbasar, "Characterization of the Clinoptilolite-Rich Tuffs of Bigadiç: Variation of the Ion-Exchange Capacity with Pretreatments and Zeolite Content," in *Proceedings of the 9th International Zeolite Conference, 5–10 July 1992, Montreal, Canada*, Vol. 2 (R. von Balmoos, J. B. Higgins, and M. M. J. Treacy, Eds.), Butterworth-Heinemann, 1993, p. 223.
17. H. Yücel and A. Culfaz, "Characterization of Clinoptilolites of Western Anatolia," in *Occurrence, Properties and Utilization of Natural Zeolites* (D. Kallo and H. S. Sherry, Eds.), Akademiai Kiado, Budapest, 1988, p. 99.
18. A. Sirkecioğlu, and A. Erdem-Şenatalar, "Estimation of the Zeolite Contents of Samples from the Bigadic Clinoptilolite Reserve," *Clays Clay Miner.*, Submitted.
19. A. Sirkecioğlu and Erdem-Şenatalar, "$CO_2$ Adsorption on Bigadiç Clinoptilolite," In Preparation.
20. R. W. Triebe, F. H. Tezel, A. Erdem-Şenatalar, and A. Sirkecioğlu, "Promising Air Purifications with Clinoptilolite," in *Volume of Recent Research Reports, 10th International Zeolite Conference, Garmisch, Germany, 1994*.
21. K. C. Khulbe, R. S. Mann, F. H. Tezel, R. W. Triebe, A. Erdem-Şenatalar, and A. Sirkecioğlu, "Characterization of Clinoptilolite by Interaction of $H_2S$, CO and $SO_2$ by ESR Technique," *Zeolites*, *14*, 481 (1994).
22. S. J. Gregg and K. S. W. Sing, *Adsorption, Surface Area and Porosity*, Academic Press, London, 1982.
23. D. T. Hayhurst, "Gas Adsorption by Some Natural Zeolites," *Chem. Eng. Commun.*, *4*, 729 (1980).
24. D. Kallo, J. Papp, and J. Valyon, "Adsorption and Catalytic Properties of Sedimentary Clinoptilolite and Mordenite from the Tokaj Hills, Hungary," *Zeolites*, *2*, 13 (1982).
25. *CRC Handbook of Chemistry and Physics*, 70th ed., CRC Press, Boca Raton, Florida, 1989.
26. K. Koyama and Y. Takeuchi, "Clinoptilolite: The Distribution of Potassium Atoms and Their Role in Thermal Stability," *Z. Kristallogr.*, *145*, 216 (1977).
27. K. S. N. Reddy, M. J. Eapen, H. S. Soni, and V. P. Shiralkar, "Sorption Properties of Cation-Exchanged β-Zeolites," *J. Phys. Chem.*, *96*, 7923 (1992).
28. C. L. Garcia and J. A. Lercher, "Adsorption of $H_2S$ on ZSM5 Zeolites," *Ibid.*, *96*, 2230 (1992).
29. H. G. Karge and J. Rasko, "Hydrogen Sulfide Adsorption on Faujasite-Type Zeolites with Systematically Varied Si–Al Ratios, *J. Colloid Interface Sci.*, *64*(3), 522 (1978).
30. H. Förster and M. Schuldt, "Infrared Spectroscopic Study of the Adsorption of Hydrogen Sulfide on Zeolites NaA and NaCaA," *Ibid.*, *52*(2), 380 (1975).

31. J. E. Huheey, *Inorganic Chemistry: Principles of Structure and Reactivity*, Harper and Row, New York, 1975.
32. M. M. Dubinin, "Physical Adsorption of Gases and Vapors in Micropores," in *Progress in Surface and Membrane Science* (D. A. Cadenhead, Ed.), Academic Press, New York, 1975, p. 1.
33. M. Suzuki, *Adsorption Engineering*, Kodansha, Tokyo, 1990.
34. R. M. Barrer and M. B. Makki, "Molecular Sieve Sorbents from Clinoptilolite," *Can. J. Chem.*, *42*, 1481 (1964).
35. R. M. Barrer, *Hydrothermal Chemistry of Zeolites*, Academic Press, London, 1982.

*Received by editor November 21, 1994*